NANO LETTERS

Letter

pubs.acs.org/NanoLett

Strain Discontinuity, Avalanche, and Memory in Carbon Nanotube Serpentine Systems

Lucas C. P. A. M. Müssnich,[†,‡] Hélio Chacham,[†] Jaqueline S. Soares,[†,§] Newton M. Barbosa Neto,[†,∥] Nitzan Shadmi,[⊥] Ernesto Joselevich,[⊥] Luiz Gustavo Cançado,[†] and Ado Jorio*[,†]

[†]Departamento de Física, Universidade Federal de Minas Gerais, Belo Horizonte, MG 31270-901, Brazil

[‡]Departamento de Física-Matemática, Instituto de Física, Universidade de São Paulo, São Paulo, SP 05314-970, Brazil

[§]Departamento de Física, Universidade Federal de Ouro Preto, Ouro Preto, MG 35400-000, Brazil

[∥]Instituto de Ciências Exatas e Naturais, Universidade Federal do Pará, Belém, PA 66075-110, Brazil

[⊥]Department of Materials and Interfaces, Weizmann Institute of Science, Rehovot, 76100, Israel

Supporting Information

ABSTRACT: This work addresses the problem of how a nano-object adheres to a supporting media. The case of study are the serpentine-like structures of single-wall carbon nanotubes (SWNTs) grown on vicinal crystalline quartz. We develop in situ nanomanipulation and confocal Raman spectroscopy in such systems, and to explain the results, we propose a dynamical equation in which static friction is treated phenomenologically and implemented as cutoff for velocities, via Heaviside step function and an adhesion force tensor. We demonstrate that the strain profiles observed along the SWNTs are due to anisotropic adhesion, adhesion discontinuities, strain avalanches, and memory effects. The equation is general enough to make predictions for various one- and two-dimensional nanosystems adhered to a supporting media.

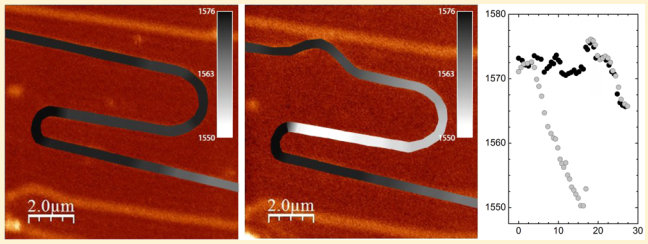

KEYWORDS: *Carbon nanotubes, nanoscale adhesion, nanotribology, Raman spectroscopy, strain, nanomanipulation*

How bulk materials transfer load to heterogeneous components immersed in the matrix is a problem that has been studied for more than 50 years.[1,2] Describing such a mechanism opens the way to understand problems of practical importance, such as the mechanical reinforcement of composites,[3−5] the design of dry adhesives,[6,7] the design of nanocircuitry for nanoelectronics,[8] and the exploitation of properties existent in graded materials to develop thermal diodes.[9] Behind such devices there is always the problem of how the systems locally adhere to the supporting media.

In the present article we study how a one-dimensional system locally interacts with a two-dimensional anisotropic surface. We use Raman spectroscopy to measure strain on single-wall carbon nanotubes (SWNTs) atop crystalline quartz that are submitted to nanomanipulation procedures. Some works have focused on the measurement of adhesion forces between carbon nanotubes and amorphous Si(SiO_2) substrates, via conventional atomic force microscopy (AFM) methods.[10,11] Other works, also using amorphous quartz substrates, have induced perturbations in long (over micrometers) SWNTs through indirect, geometrically induced deformations,[12] or via direct nanomanipulation with the aid of an AFM apparatus.[13,14] The system we study here is more complex than previously studied ones in two ways: first, the nanotube is sitting on crystalline quartz, that exhibits anisotropic interaction with the nanotubes, depending on the direction that the nanotube is deposited with respect to the crystalline structure; second, the crystal structure and the growth process generate what has been called SWNT serpentines, where one SWNT is deposited with parallel segments connected by U-turns, in a serpentine-like geometry,[15] thus generating changes in the tube-substrate interaction along the SWNT.

The dynamics behind the formation of such complex structures have been successfully described using multimillion fully atomistic molecular dynamics simulations.[16] However, we have extensively applied Raman spectroscopy to locally probe strain in the SWNTs[17−19] and we detected a variety of different and complex local SWNT-substrate interactions, which could not be captured by the analysis performed in ref 16. To fully understand the complexity of the tube-substrate interaction of the quasi-one-dimensional SWNTs with the crystalline quartz, we apply here well-designed nanomanipulation procedures with in situ Raman spectroscopy measurements to study results of the system's dynamics. We developed a mechanical model for the elastodynamics of a line system in a frictive media and used it to infer the system's elastostatics. Our model is the first to analytically reveal already reported experimental behavior,[12,13] and it also describes how that "fixed points" can induce

Received: May 20, 2015
Revised: July 27, 2015
Published: July 30, 2015

DOI: 10.1021/acs.nanolett.5b01982
Nano Lett. 2015, 15, 5899−5904

characteristic strain profiles, easily recognizable in experiments, as well as that successive perturbations on the same system generate "avalanche-like" profiles resembling self-organized patterns,[20] that remain written in the SWNT spectroscopic strain-related response, demonstrating memory effects.

Figure 1 shows three examples of SWNT serpentines that were nanomanipulated using AFM tips. The images are

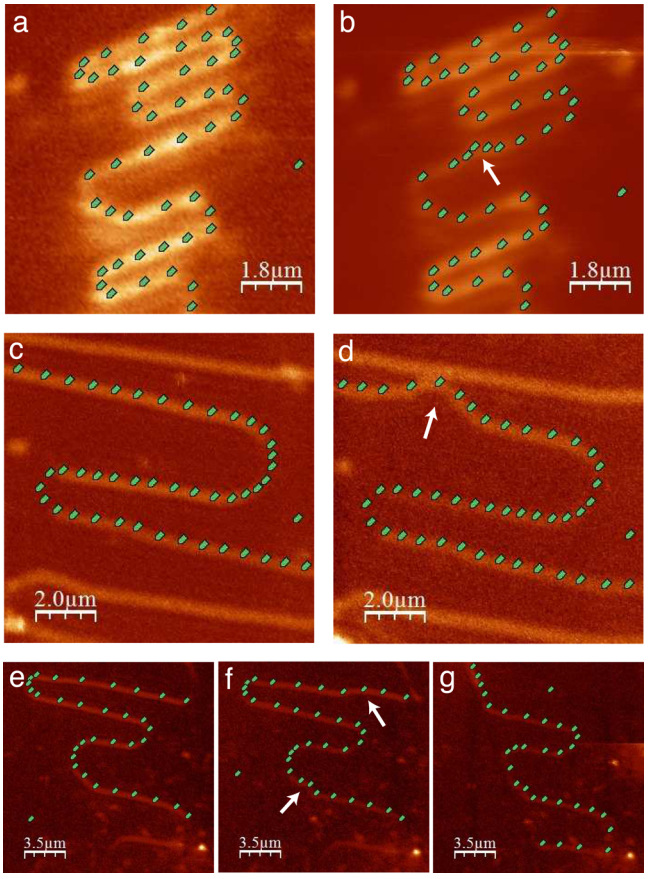

Figure 1. Confocal G-band Raman intensity from SWNTs sitting on vicinal crystalline quartz. Panels a and b stand for one SWNT measured before and after nanomanipulation, respectively. Panels c and d stand for the second SWNT measured before and after nanomanipulation, respectively. Panels e, f, and g display the third experiment, where the same SWNT was nanomanipulated twice, in the sequence. White arrows point to the locations where the nanomanipulations occurred. The green pointers show the locations where Raman spectra were taken and are analyzed in Figure 2. Green pointers out of the serpentines are reference data to ensure the substrate does not interfere in the analysis.

obtained by confocal Raman spectroscopy, where the colors indicate the intensity of the SWNT C−C stretching mode (called G-band, at ∼1590 cm^{-1}).[21−23] The growth procedure of the SWNT serpentines and the experimental apparatus used for the in situ nanomanipulation-spectroscopy measurements have been described elsewhere (see refs 15 and 24 respectively). In this study, nanomanipulation is always a process of touching the substrate with the AFM tip nearby a SWNT segment, and then pushing it with the tip, perpendicularly to the tube axis. It is important to comment that we always succeeded to manipulate the SWNT serpentines when pushing them perpendicularly to the straight segments, while we failed in all our efforts to push a serpentine in the U-turn segments, perpendicularly to the tube axis at those locations. In total, we have studied the G-band profile of 34 SWNT serpentines, while in four cases we applied nanomanipulation procedures. In one case we performed one nanomanipulation procedure, two nanomanipulations in two cases, while in the fourth we performed 10 successive nanomanipulation procedures.

In Figure 1, a and b stand for the same SWNT measured before and after nanomanipulation, respectively. The nanomanipulation took place at the central part of the figure, and it can be seen in Figure 1b by a local misalignment of the central straight SWNT segment. The green pointers show the locations where Raman spectra were taken for further analysis (Figure 2).

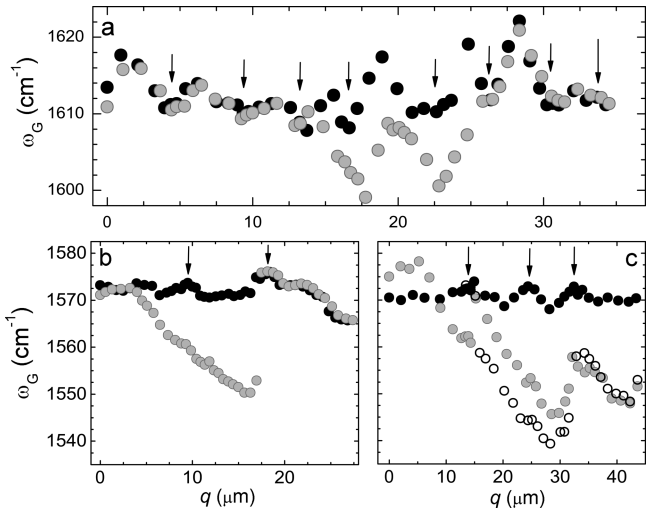

Figure 2. G-band Raman frequency (ω_G) from SWNTs sitting on vicinal crystalline quartz. The ω_G obtained from the green pointer locations in Figure 1a−b, c−d, and e−g are shown here in panels a, b, and c, respectively. Black, gray, and white circles stand for the results from the nonmanipulated SWNT, SWNT after first nanomanipulation, and SWNT after the second nanomanipulation, respectively. The circles are sized according with the uncertainty in frequency. The arrows point to the center of the serpentine U-turns.

Figures 1c, d show another nanomanipulated SWNT, again before (c) and after (d) the procedure. Here the location where nanomanipulation happened is more pronounced than in Figure 1b, appearing in Figure 1d as the local misalignment of the previously straight SWNT segment (compare with Figure 1c). Finally, Figures 1e, f, and g display the third experiment, where the same serpentine was nanomanipulated twice in sequence. Figure 1e is the nonmanipulated structure. Figure 1f shows the result after the first nanomanipulation procedure. Careful analysis of Figure 1f shows that the tube was displaced in two locations, one at the central part of the figure (intentional), and the other at the end of the top straight segment (nonintentional). The second nanomanipulation procedure, shown in Figure 1g, was a strong pushing procedure, and the entire top straight segment was moved.

SWNTs usually exhibit two G-band features, named G^+ (strong) and G^- (weak).[21−23] The analysis discussed now is based on the G^+ band frequency obtained at specific SWNT locations, as indicated by the green pointers in Figure 1. The results are displayed in Figure 2. Local changes in the G-band frequency (ω_G) are known to be proportional to local changes in strain.[12,13,21,22,25] A decrease in ω_G reflects an increase in the local strain. Figure 2a shows the G-band frequency before

DOI: 10.1021/acs.nanolett.5b01982
Nano Lett. 2015, 15, 5899−5904

(black bullets) and after (gray bullets) nanomanipulation on the SWNT shown in Figure 1a,b, respectively, obtained at the locations indicated by the green pointers. The arrows in Figure 2 point to the center of the serpentine U-turns, and the ω_G variations in the SWNT before nanomanipulation (black bullets) are due to different local strains resulting from the growth procedure itself, as discussed in ref 17. The result of ω_G after nanomanipulation is shown by the gray bullets, the nanomanipulation procedure having taken place around $q \sim 20$ μm. It is similar to what has been reported previously,[13] revealing a local ω_G variation in a W-shaped pattern. The length of strain propagation (10 μm) is 4 orders of magnitude larger than the tube diameter ($d_t \sim 1$ nm, measured by AFM), and the slope of each of the straight segments in the W ($\Delta\omega_G/\Delta q$) gives a measure of the local strain adhesion force, as discussed in ref 13 and predicted by the theoretical treatment below. As we will show, the W-shape is due to homogeneous adhesion between SWNT and the substrate.

Figure 2b shows a similar analysis for the second experiment (displayed in Figure 1c,d), focusing on one side of the W shape, where a different behavior is observed, which is an abrupt change in ω_G (or strain) at $q \sim 17$ μm. The nanomanipulation happened at $q \sim 0$, and the strain along one direction propagates ($\Delta\omega_G$) for about 17 μm, when it abruptly goes to zero. As shown later, this result evidence the presence of a portion of the SWNT that is strongly fixed to the substrate, through which strain cannot propagate any further—hence the name "fixed point". Similar behavior has been observed in different cases, in both nanomanipulated (this work) and nonmanipulated samples,[18,19] and in all cases it happens at the starting of a U turn, where the carbon nanotube detaches from a straight segment (see more details about the substrate structure in refs 15 and 16).

Finally, Figure 2c shows the most complex case, where the SWNT was nanomanipulated twice. The black, gray, and white bullets show ω_G in the sample before nanomanipulation, after the first nanomanipulation procedure, and after the second nanomanipulation procedure, respectively. As commented before, the second nanomanipulation procedure was strong enough to detach and to displace the entire segment (see Figure 1g). What is remarkable here is the difference between the results after the first and the second nanomanipulations. Notice the change in ω_G that goes from $q \sim 15$ μm to $q \sim 30$ μm. The frequency drops rigidly by about 10 cm^{-1}, without changing the slope $\Delta\omega_G/\Delta q$. As discussed below, this rigid drop is related to strain effects caused by the second push, hence the name "strain avalanche". The final strain distribution, evidenced here by the white bullets in Figure 2c, reflects the memory of the system, which had been strained during its growth process and subsequently by a nanomanipulation procedure in which it was twice perturbed.

The mechanical model devised to explain the observed phenomena is a continuous elastic line system in two dimensions, immersed in a viscous frictive media, which is deformed and then let relax to a stationary state. It is constrained to three experimental facts: strong elastic regime (SWNT's high Young's modulus[26]); strong viscous regime (small displacement of the serpentines after nanomanipulation); and adhesion as a cutoff for the dynamics (serpentines in nonequilibrium stationary states with little or no relaxation after long elapsed times, such as months). The proposed equation is

$$\frac{1}{\nu}\frac{\partial \mathbf{u}}{\partial t}(q,t) = \mathbf{f}(q,t)\Theta(f(q,t) - |\vec{f}_{adh}(q,t)\cdot\hat{f}(q,t)|) \quad (1)$$

Here t is time; q is a parametrization for the line system's points prior to being deformed; $\mathbf{u}$ is the deformation vector of the system at point q and time t, with $\partial\mathbf{u}/\partial t$ its velocity; $1/\nu$ is the viscosity of the medium, related to an isotropic viscous frictive force due to the velocity of the system. $\mathbf{f}(q,t)$ is the elastic force per unit length acting on point q and at time t, $f(q,t) = |\mathbf{f}(q,t)|$ and $\hat{f}(q,t) = \mathbf{f}(q,t)/f(q,t)$. $\mathbf{f}(q,t)$ is given by

$$\mathbf{f}(q,t) = YA\left(\frac{\partial s(q,t)}{\partial q}\hat{t}(q,t) + s(q,t)\frac{\partial \hat{t}(q,t)}{\partial q}\right) \quad (2)$$

in which Y is the system's Young's modulus; A is the system's cross sectional area; s is the continuous axial strain field of the system, with respect to equilibrium, and $\hat{t}$ is the unit vector tangent to the line system at each point q and time t. Finally, Θ is Heaviside's step function, and $\vec{f}_{adh}$ represents the adhesion force tensor between the line system and the medium, in units of force per unit length, which might depend upon position q and time t.

Inextricably intertwined to the model are the parameters related to boundary conditions. These are $\mathbf{v}$, t_{nano}, C, l_{step}. The reason is that the model reproduces the nanomanipulation procedure to which the serpentines were submitted, as well as the anisotropic nature of the vicinal crystalline quartz substrate over which they were deposited. Nanomanipulation is modeled by imposing, initially, the nonzero velocity $\mathbf{v}$ to a portion of the system for an amount of time specified by t_{nano}, after which the system is governed solely by eq 1, and anisotropy is modeled through the adhesion force tensor $\vec{f}_{adh}$, which, if the Cartesian y direction is chosen as the one perpendicular to the quartz steps, acquires the diagonal form

$$\vec{f}_{adh} = \begin{pmatrix} f_{adh}^{xx} & 0 \\ 0 & f_{adh}^{yy} \end{pmatrix} \quad (3)$$

so C is defined as the ratio $f_{adh}^{yy}/f_{adh}^{xx}$ at the position of the quartz step, which is a stripe of length l_{step} parallel to x direction.

To test the model, eq 1 together with the appropriate boundary conditions were numerically simulated. For this purpose, a discretized version of 1 was obtained, and a direct correspondence between the macroscopic parameters of 1 and the microscopic parameters thus derived was established (see Supporting Information). Two features were carefully observed: (i) the identification of the parameters that could be related to experiment, and (ii) the sensitivity of the simulations on those parameters that could not, called free parameters. Regarding (i), it was first supposed that, throughout the serpentines, the expression

$$\Delta\omega = c_1 s \quad (4)$$

relating variation in Raman frequency to strain is valid, with c_1 a constant for each serpentine,[25] $\Delta\omega = \omega - \omega_o$, ω_o the system's Raman frequency before it receives the strain load described by s (supposed constant), and ω the system's Raman frequency after. Second, we defined c_2: $= f_{adh}^{xx}/YA$ and, third, we supposed that, after the nanomanipulation procedure, $\Delta\omega(q) = c_3 q$. Thus, it can be shown that, for the experimental data to be reproduced by the model, one must have

DOI: 10.1021/acs.nanolett.5b01982
Nano Lett. 2015, 15, 5899−5904

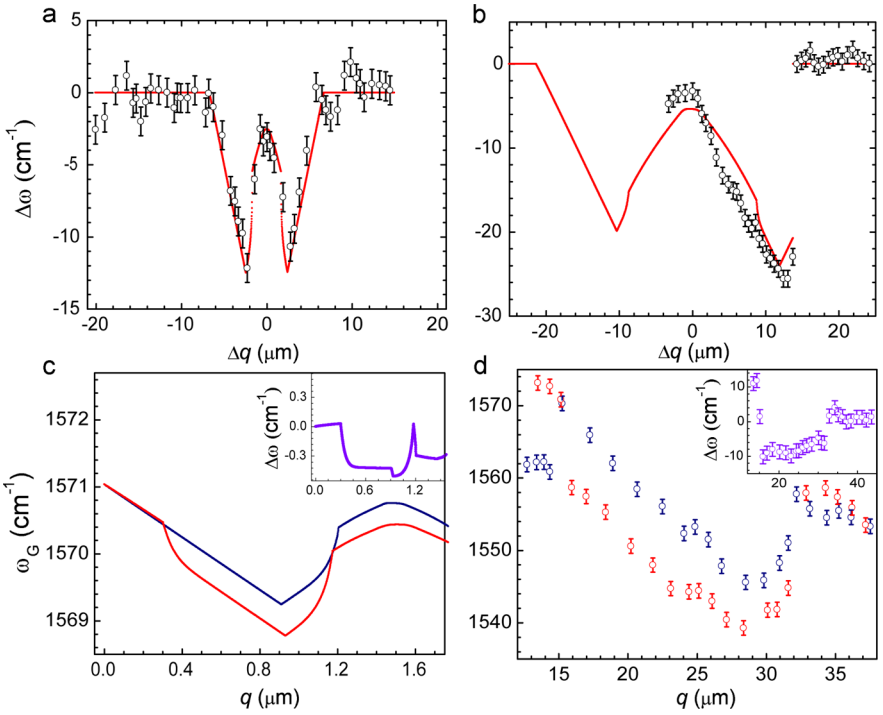

Figure 3. Results of numerically simulating eq 1, for optimal choices of boundary conditions (free parameters). (a) Comparison between theory (red dotted line) and experiment (open circles with error bars) for the serpentine depicted in Figure 1a,b and in Figure 2a. (b) Comparison between theory and experiment for serpentine depicted in Figure 1c,d and in Figure 2b. (c) and (d) make a qualitative comparison between theory and experiment for the serpentine depicted in Figure 1e−g and in Figure 2c. (c) stands for a theoretical reproduction of the effect seen in the detailed region of (d). The insets at upper right-hand corners of (c) and (d) display the differences between the profiles in the main plot. As in a and b, inset of d involved interpolation to allow the point by point subtraction.

$$c_2 = \frac{c_3}{c_1} \tag{5}$$

and this ties f_{adh}^{xx}, Y and A to the experiments (see Supporting Information). The other parameter that can be related to experiments is the total length of the numerical system, L, since the physical length of the affected region of the serpentines, $\mathcal{L}$, which can be measured by the confocal images in Figure 1, requires $L \geq \mathcal{L}$.

Regarding (ii), the free parameters happened to be the ones that determine the boundary conditions, that is, $\mathbf{v}$, t_{nano}, C, and l_{step}. Numerical simulations varying them were performed, and the values that optimized strain profiles versus spatial displacement of the line system were selected to adjust the data (more details in the Supporting Information). The parameter ν is not essential to the model, since it can be properly removed by a time rescaling.

Representative results of the above-mentioned numerical simulations are shown in Figure 3. In all cases, results are displayed not as the strain field s, but rather as Raman G^+ variation curves, obtained with the use of eq 4. The spatial coordinates q are supposed to be that of the line system's prior to being deformed. In Figure 3a and b, $\Delta q = 0$ μm is the position at which nanomanipulation took place, both theoretically and experimentally, and experimental data (open circles with error bars) depict the difference $\Delta\omega$ between Raman G^+ frequency before and after nanomanipulation, which was obtained through point by point subtraction of values (with the aid of interpolation) for the regions not affected by nanomanipulation, and through subtraction of a chosen ω_o value for the affected regions. This procedure considers the assumption that nanomanipulation was enough to erase memory from growth-induced strain.

Figure 3a depicts the theoretical model (dotted red lines) fitting the experimental data (open circles with error bars) relative to the simplest case shown in Figure 1a,b and 2a. Agreement is excellent, both qualitative and quantitative. Experimentally related parameters had values $c_1 = -497.5$ cm^{-1}, $c_3 = -2.97$ cm^{-1}/μm, so that $c_2 = 0.0060$ μm^{-1}, and we chose $\omega_o = 1611.2$ cm^{-1}. One can observe the essential qualitative features discussed above and in the literature:[12,13] the typical W shape in the Raman G^+ variation curve, with constancy of its slope. This constancy, however, is present only when adhesion is homogeneous. Where it is not, we observe nonanalytical behavior of the Raman G^+ variation curve of the system. In this case, this happens close to the region at which it detaches from the step, called the detachment region (around +2.0 and −2.0 μm, approximately). This becomes physically relevant when we notice that the result generated with $C = 1$ (that is, the case of no discontinuity in adhesion) does not fit experimental results so well within the experimental error (see Supporting Information). To the best of our knowledge of the literature, this seems to be a prediction about an indeed novel nanotribological feature, generated by the inhomogeneous adhesion induced by the anisotropic character of the substrate.

Figure 3b shows an attempt to fit experimental data from Figure 1c,d and 2b. Experimentally related parameters had values $c_1 = -517.4$ cm^{-1}, $c_3 = -1.84$ cm^{-1}/μm, so that $c_2 = 0.0036$ μm^{-1}, and we chose $\omega_o = 1575.8$ cm^{-1}. The qualitative features from the previous case (W shape, constancy of slope, and nonanalyticity) discussed above can be observed. The novel feature that emerges, though, is the above-mentioned

DOI: 10.1021/acs.nanolett.5b01982
Nano Lett. 2015, 15, 5899−5904

"fixed-point" effect: we imposed that the portion of the system at q_o = 13.75 μm should have, as boundary condition, zero velocity for all times. Because of eq 1, this resulted in strain not propagating to regions further than q_o, leading to an abrupt discontinuity in the Raman G^+ variation curve. For this reason, q_o was called a "fixed-point" for the system. Figure 3b suggests that this is the cause for what is indeed observed in the experimental data. We physically interpret this fact as a limiting case of strong, discontinuous adhesion between the carbon serpentine and the vicinal quartz substrate: for strain to trespass a fixed-point, arbitrarily large force per unit length must be done. This might explain our failure in pushing the serpentines in the U-turn segments, perpendicularly to the tube axis.

Finally, Figure 3c shows a theoretical reproduction of the novel qualitative features brought in by the most complex experimental data from Figure 1e,f,g and 2c,d, where the relevant region for analysis is the one given in detail in Figure 3d. Experimentally related parameters had values c_1 = −907.2 cm^{-1}, c_3 = −2.00 cm/μm, so that c_2 = 0.0022 μm^{-1}, and we chose ω_o = 1571.0 cm^{-1}. The region between 0.4 μm and 1.2 μm in Figure 3c makes a direct parallel to the region between 15 μm and 33 μm in Figure 3d: in both cases, subsequent nanomanipulations in analog places produce new Raman G^+ variation curves which are almost uniformly displaced relative to the initial ones. Theoretically, eqs 1 and 4 show that this equals a uniform displacement in strain, whence the term "strain avalanche". The insets at the upper right-hand corners of Figure 3c, d confirm the strain avalanches by depicting the difference between the final and initial plots. The constant values of displacement were around −0.4 cm^{-1}, for the theoretical case, and around −10 cm^{-1}, for the experimental case. Furthermore, the observation of the strain avalanche has an immediate consequence: it implies that previous stationary states are starting point for subsequent dynamics, or, in other words, that the serpentine-vicinal quartz substrate is a system with memory due to nanotribological effects. The fitting values for the three serpentines are displayed in Table 1 for easy comparison of the fitting values.

Table 1. Values of ω_0, c_1, c_2, and c_3 Obtained by Fitting the Data from Serpentines 1 (Figure 1a,b), 2 (Figure 1c,d), and 3 (Figure 1e,f,g)

serpentine	ω_0 (cm^{-1})	c_1 (cm^{-1})	c_2 (μm^{-1})	c_3 (cm^{-1} /μm)
1	1611.2	−497.5	0.0060	−2.97
2	1575.8	−517.4	0.0036	−1.84
3	1571.0	−907.2	0.0022	−2.00

Notice that our analysis is fully devoted to uniaxial strain, while Duan et al.[13] reported the effect of both uniaxial strain and torsional strain on the Raman frequency of nanomanipulated carbon nanotubes. In our case, extensive uniaxial strain is the main type considered because (i) we did not observed changes in the carbon nanotube radial breathing mode frequencies, and (ii) the length scale of the propagation of perturbations is much greater than the diameter of the tube and than the perturbed region. Nonetheless, the gray bullets in Figure 2c present a region (a plateau close to $q \sim 0$ μm) in which there might be compressive uniaxial strain or torsional strain (because of the increase in ω_G and because it is the perturbed region). This region becomes detached from the substrate after the second nanomanipulation procedure, and therefore only extensive uniaxial strain would remain for the final strain profile. We also neglect the possibility that the spectral changes we observe could have been due to damages introduced in the nanotubes by the nanomanipulation procedure, since Raman spectroscopy is well-known as the most sensitive technique to sense defects in graphene-related structures,[27−29] and the presence of defect-induced peaks are not observed in our study.

In summary, we have identified here the important role played by adhesion anisotropy and discontinuity, strain avalanche, and memory in the strain profiles measured in carbon serpentine systems. These results can be generally applied for one-dimensional systems sliding on a two-dimensional surface, and the main ideas can be extended to one-dimensional systems immersed in a three-dimensional medium or to two-dimensional nanosystems on a surface, i.e., to general friction problems in nanotribology. Recent experiments show strain gradients for graphene sitting on a surface,[30−34] indicating that the dynamical model presented here can be readily extended to two-dimensional systems like graphene, phosphorene, hexagonal-BN, or transition metal dichalcogenides sitting on surfaces.

■ ASSOCIATED CONTENT

Supporting Information

The Supporting Information is available free of charge on the ACS Publications website at DOI: 10.1021/acs.nanolett.5b01982.

Discretized version of eq 1 for numerical simulations; derivation of eq 5; comment on the implementation of the code; sensitivity of the numerical simulations to the free parameters of the model (PDF)

Code for numerical simulations (PDF)

■ AUTHOR INFORMATION

Corresponding Author

*Phone: +55 31 34096610. Fax: +55 31 34095600. E-mail: adojorio@fisica.ufmg.br.

Notes

The authors declare no competing financial interest.

■ ACKNOWLEDGMENTS

This work was financed by CNPq (grant 552124/2011-7).

■ REFERENCES

(1) Cox, H. *Br. J. Appl. Phys.* **1952**, *3*, 72.
(2) Haque, A.; Ramasetty, A. *Composite Structures* **2005**, *71*, 68−77.
(3) Thostenson, E.; Li, W.; Wang, D.; Ren, Z.; Chou, T. *J. Appl. Phys.* **2002**, *91*, 6034−6037.
(4) Thostenson, E. T.; Li, C.; Chou, T.-W. *Compos. Sci. Technol.* **2005**, *65*, 491−516.
(5) Rodriguez, A. J.; Guzman, M. E.; Lim, C.-S.; Minaie, B. *Carbon* **2011**, *49*, 937−948.
(6) Veedu, V. P.; Cao, A.; Li, X.; Ma, K.; Soldano, C.; Kar, S.; Ajayan, P. M.; Ghasemi-Nejhad, M. N. *Nat. Mater.* **2006**, *5*, 457−462.
(7) Qu, L.; Dai, L.; Stone, M.; Xia, Z.; Wang, Z. L. *Science* **2008**, *322*, 238−242.
(8) Yarden, T. S.; Joselevich, E. *Nano Lett.* **2010**, *10*, 4742−4749.
(9) Pereira, E. *Phys. Rev. E* **2011**, *83*, 031106.
(10) McElroy, K.; Davis, R. C.; Hawkins, A. *Appl. Phys. Lett.* **2007**, *91*, 233119−233119.
(11) Whittaker, J. D.; Minot, E. D.; Tanenbaum, D. M.; McEuen, P. L.; Davis, R. C. *Nano Lett.* **2006**, *6*, 953−957.

DOI: 10.1021/acs.nanolett.5b01982
Nano Lett. 2015, 15, 5899−5904

(12) Son, H.; Samsonidze, G. G.; Kong, J.; Zhang, Y.; Duan, X.; Zhang, J.; Liu, Z.; Dresselhaus, M. S. *Appl. Phys. Lett.* **2007**, *90*, 253113.
(13) Duan, X.; Son, H.; Gao, B.; Zhang, J.; Wu, T.; Samsonidze, G. G.; Dresselhaus, M. S.; Liu, Z.; Kong, J. *Nano Lett.* **2007**, *7*, 2116−2121.
(14) Yano, T.-A.; Ichimura, T.; Kuwahara, S.; H'Dhili, F.; Uetsuki, K.; Okuno, Y.; Verma, P.; Kawata, S. *Nat. Commun.*. **2013**, *4*, 10.1038/ncomms3592
(15) Geblinger, N.; Ismach, A.; Joselevich, E. *Nat. Nanotechnol.* **2008**, *3*, 195−200.
(16) Machado, L.; Legoas, S.; Soares, J.; Shadmi, N.; Jorio, A.; Joselevich, E.; Galvão, D. *Phys. Rev. Lett.* **2013**, *110*, 105502.
(17) Soares, J. S.; et al. *Nano Lett.* **2010**, *10*, 5043−5048.
(18) Soares, J. S.; Barros, E. B.; Shadmi, N.; Joselevich, E.; Jorio, A. *Phys. Status Solidi B* **2011**, *248*, 2536−2539.
(19) Soares, J. S.; Jorio, A. *J. Nanotechnol.* **2012**, *2012*, 1; 10.1155/2012/512738
(20) Whitesides, G. M.; Grzybowski, B. *Science* **2002**, *295*, 2418−2421.
(21) Reich, S.; Thomsen, C.; Maultzsch, J. *Carbon nanotubes: basic concepts and physical properties*; John Wiley & Sons: New York, 2008.
(22) Jorio, A.; Dresselhaus, M. S.; Saito, R.; Dresselhaus, G. *Raman spectroscopy in graphene related systems*; John Wiley & Sons: New York, 2011.
(23) Saito, R.; Hofmann, M.; Dresselhaus, G.; Jorio, A.; Dresselhaus, M. *Adv. Phys.* **2011**, *60*, 413−550.
(24) Araujo, P.; Barbosa Neto, N.; Chacham, H.; Carara, S.; Soares, J.; Souza, A.; Cançado, L.; De Oliveira, A.; Batista, R.; Joselevich, E.; Dresselhaus, M. S.; Jorio, A. *Nano Lett.* **2012**, *12*, 4110−4116.
(25) Reich, S.; Jantoljak, H.; Thomsen, C. *Phys. Rev. B: Condens. Matter Mater. Phys.* **2000**, *61*, R13389.
(26) Yamamoto, T.; Watanabe, K.; Hernández, E. R. *Carbon nanotubes: Advanced Topics in the Synthesis, Structure, Properties and Applications*; Springer: New York, 2008; pp 165−195.
(27) Pimenta, M.; Dresselhaus, G.; Dresselhaus, M. S.; Cancado, L.; Jorio, A.; Saito, R. *Phys. Chem. Chem. Phys.* **2007**, *9*, 1276−1290.
(28) Maciel, I. O.; Anderson, N.; Pimenta, M. A.; Hartschuh, A.; Qian, H.; Terrones, M.; Terrones, H.; Campos-Delgado, J.; Rao, A. M.; Novotny, L.; Jorio, A. *Nat. Mater.* **2008**, *7*, 878−883.
(29) Archanjo, B.; Maciel, I.; Ferreira, E. M.; Peripolli, S.; Damasceno, J.; Achete, C.; Jorio, A. *Ultramicroscopy* **2011**, *111*, 1338−1342.
(30) Gong, L.; Kinloch, I. A.; Young, R. J.; Riaz, I.; Jalil, R.; Novoselov, K. S. *Adv. Mater.* **2010**, *22*, 2694−2697.
(31) Kitt, A. L.; Qi, Z.; Ret'mi, S.; Park, H. S.; Swan, A. K.; Goldberg, B. B. *Nano Lett.* **2013**, *13*, 2605−2610.
(32) Androulidakis, C.; Koukaras, E. N.; Frank, O.; Tsoukleri, G.; Sfyris, D.; Parthenios, J.; Pugno, N.; Papagelis, K.; Novoselov, K. S.; Galiotis, C. *Sci. Rep.* **2014**, *4*, 5271.
(33) Beams, R.; Cançado, L. G.; Jorio, A.; Vamivakas, A. N.; Novotny, L. *Nanotechnology* **2015**, *26*, 175702.
(34) Merijntje, S. B.; et al. *Nano Lett.* **2015**, *15*, 147; 10.1021/nl503246h

DOI: 10.1021/acs.nanolett.5b01982
Nano Lett. 2015, 15, 5899−5904